

PRELIMINARY RELATIVE PERMEABILITY ESTIMATES OF METHANE HYDRATE-BEARING SAND

Yongkoo Seol, Timothy J. Kneafsey, Liviu Tomutsa, and George J. Moridis

Lawrence Berkeley National Laboratory
Berkeley, CA. 94702, USA
E-mail: yseol@lbl.gov

ABSTRACT

The relative permeability to fluids in hydrate-bearing sediments is an important parameter for predicting natural gas production from gas hydrate reservoirs. We estimated the relative permeability parameters (van Genuchten α and m) in a hydrate-bearing sand by means of inverse modeling, which involved matching water saturation predictions with observations from a controlled waterflood experiment. We used x-ray computed tomography (CT) scanning to determine both the porosity and the hydrate and aqueous phase saturation distributions in the samples. X-ray CT images showed that hydrate and aqueous phase saturations are non-uniform, and that water flow focuses in regions of lower hydrate saturation. The relative permeability parameters were estimated at two locations in each sample. Differences between the estimated parameter sets at the two locations were attributed to heterogeneity in the hydrate saturation. Better estimates of the relative permeability parameters require further refinement of the experimental design, and better description of heterogeneity in the numerical inversions.

INTRODUCTION

The thermal conductivity, permeability, and relative permeabilities of liquid and gas through hydrate-bearing sediments are needed when conducting numerical simulations of gas production from gas hydrate reservoirs. Field measurements and laboratory studies can provide reasonably accurate estimates for the thermal conductivity of the sediment/hydrate/water/gas medium (Kneafsey et al., 2005). The absolute permeability and the relative permeabilities to gas and water flow can be obtained using laboratory measurements.

Relative permeability measurements of hydrate-bearing sediments using the traditional technique of simultaneously injecting the phases of interest (gas and water) into a sample are complicated because this would typically cause the formation of new hydrate, thus affecting flow paths and permeability. In the waterflood technique, however, only water is injected. This technique was selected to minimize additional hydrate formation by limiting the gas available for hydrate formation.

X-ray computed tomography (CT) allows visualization of the distribution of hydrate, liquid and

gas phases in a sample, and provides a quantification of the saturation for each system component in real time (Tomutsa et al., 2002). CT also aids in understanding how the hydrate forms and how water flows through hydrate-bearing sediments.

We formed methane hydrate in the pore space of tightly packed fine sand under moderate pressure and temperature conditions. Gas permeabilities were measured before and after the hydrate formation, and a water flow-through test (waterflood) was performed while the sample was being monitored by x-ray CT scanning to aid in estimating the relative permeabilities in the hydrate-bearing sample. The relative permeability was determined by inverting the experimental data using the iTOUGH2 code (Finsterle, 1999).

METHODS

Laboratory Experiments

The experimental setup is shown in Figure 1. Sand samples (37.8 mm diameter, 90 mm length) in the rubber sleeve were placed under triaxial confining pressure inside an aluminum pressure vessel, surrounded by a water jacket for temperature control. Temperature was monitored through thermocouples inside the sample and in the water jacket, and pressure is continuously recorded with pressure transducer at both ends. A modified medical Siemens Somatom HI Q Computed Tomography scanner was used to monitor the sample.

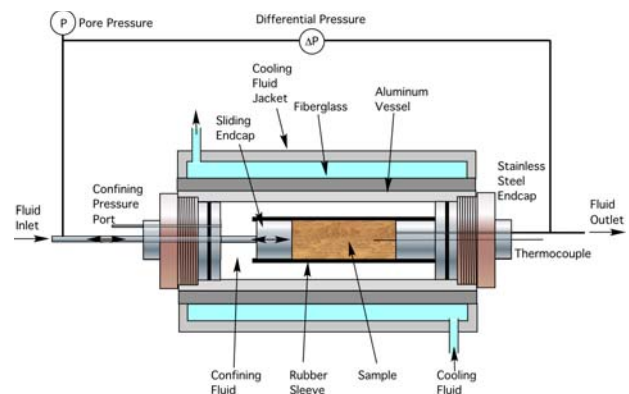


Figure 1. System schematic.

Determination of the relative permeability of a hydrate-bearing medium included the following steps:

- Packing the moistened sand sample into the pressure vessel sleeve, and making an initial gas permeability measurement
- Converting sample water into hydrate
- Measuring the gas permeability of the hydrate-bearing system
- Injecting water (waterflooding) while monitoring saturation changes at fixed locations
- Inducing hydrate dissociation and making a single-phase (gas or water) permeability measurement of the sand without the hydrate.

Temperatures and pressures were measured and recorded at a number of sample locations during the tests. The x-ray CT data were used to describe the initial packing, the initial water distribution, the hydrate distribution, and the paths where water flowed through the hydrate-bearing sediment. Full-sample scans were performed at critical junctures, e.g., at the beginning of a test, after hydrate formation, and when the samples were water-saturated or dried. During waterflooding, the saturation changes at selected sample locations were monitored by x-ray CT scanning.

Sand Pack and Gas Permeability Measurements

The silica sand used in this study was moistened in a stepwise manner to predetermined moisture contents (Table 1), with sufficient mixing to homogenize the sample. The moistened sand was tamped into the sleeve (Figure 1) using a 1.27 cm diameter rod with about 100 blows per lift after first placing a 0.32 cm diameter tube over the thermocouple to protect it from the tamping. To check the sleeve for leaks, the confining pressure was set to 2.75 MPa (without increasing the pore pressure) and held for up to 12 hours. As a final compaction step, the confining pressure was raised to 4.17 MPa for several minutes, and then lowered to 2.75 MPa. During the tests, the effective stress (confining pressure minus pore pressure) was maintained near 2.75 MPa, and always below 4.17 MPa.

Gas permeability was measured by applying gas flow through the sample and by measuring the pressure drop across the sample. Multiple flow rates were used in each measurement. Computations of gas permeability were performed using the known gas density and viscosity at the test conditions, and when applicable by considering the variation in gas density across the sample.

Hydrate Formation

Methane hydrate was formed by changing the pore methane pressure and temperature within the sample to conditions where the hydrate is stable ($P = 4.5501 \times 10^6$ Pa, and $T = 3.5$ °C). Hydrate typically started forming soon after the stability condition was reached and was generally completed within 12 hours. The hydrate saturation S_H was initially non-uniform, as can be seen in Figure 2, which shows the hydrate saturation in the 18 consecutive images for entire sample (Each slice is 5 mm thick). The heterogeneity in S_H was attributed to capillary pressure increases as hydrate forms, inducing water migration towards the forming hydrate.

We conducted three tests using samples with varying initial water saturations (19 to 53%; see Table 1) under the similar pressure and temperature conditions. The pattern of hydrate formation varies with each test. In Test 1, large regions that are nearly fully hydrate saturated occurred towards the downstream end of the sample. These tended to focus water flow through the less saturated zones. In Test 2, hydrate concentrated dominantly in a region near the sample center. In Test 3 a more uniform hydrate saturation was achieved, probably because of the lower initial water content relative to the first two tests.

Following hydrate formation, gas permeability of the hydrate-bearing sample was determined flowing gas through the sample while measuring the pressure difference across the core.

Table 1. Test conditions

Test	Porosity / Standard Deviation	Water Sat./ Standard Deviation	Hydrate Conv.	Hydrate Sat./ Standard Deviation
1	0.39/0.01	0.53/0.08	100%	0.68/0.15
2	0.39/0.01	0.41/0.04	100%*	0.57/0.19
3	0.39/0.01	0.19/0.02	86%	0.26/0.03

*Calculations indicated that more than 100% conversion occurred, indicating a leak over the core.

Waterflood with CT Observation

To gain information on the flow behavior of water in the hydrate-bearing sediments, we performed a waterflood experiment for each of the three conditions investigated (Table 1). Water was injected at a fixed rate of 0.1 mL/min (Test 1) or 0.2 mL/min (Tests 2 and 3). Two locations that had more uniform hydrate distributions or features of interest were selected in each test to estimate water saturation by CT scanning. These locations are indicated in Figure 2.

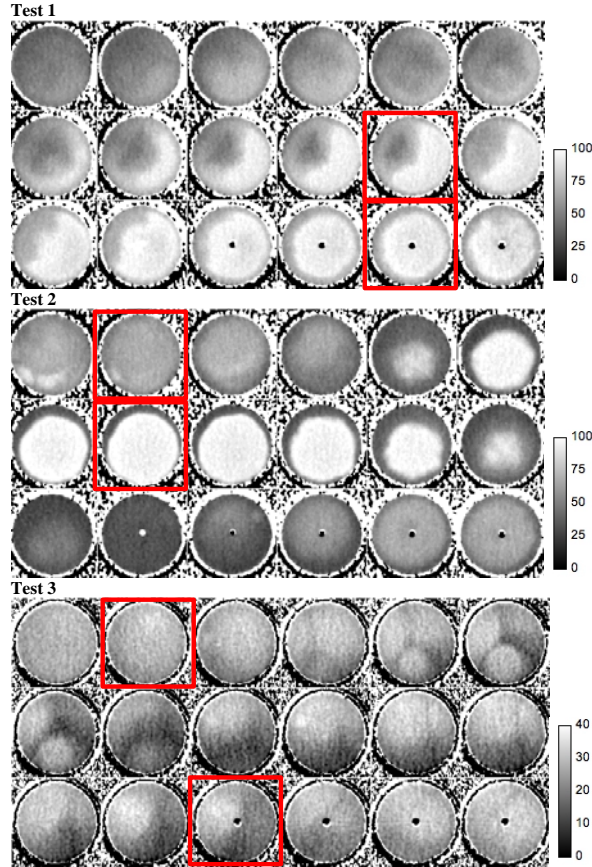


Figure 2. Pre-waterflood hydrate saturations (%) in the three tests: Locations monitored during the waterfloods are identified by red boxes. The fluid injection port is located in the vicinity of the upper left image, while the flow outlet is located in the lower right image.

Hydrate Dissociation, Sample Saturation, and Drying

Following the waterfloods, we induced hydrate dissociation by warming the samples, and the samples were then saturated with water. The water saturation was performed by first flowing CO_2 gas through the sample, then flushing with water, and finally pressurizing water to dissolve remaining CO_2 gas. While the sample was water saturated, the permeability was measured by flowing water at a known rate through the sample and measuring the pressure differential across the sample. The sample was then dried by flowing dry nitrogen gas through the sample. CT scans for entire sample were performed at both water saturated and dried states to provide reference conditions for calculating local saturation values.

Numerical Simulation Studies

Model Development

A one-dimensional (1-D) model was developed based on the actual dimensions of the sample. The actual measurements of the core dimensions were provided by analysis of x-ray CT images using ImageJ[®].

For the modeling, we assumed that the sand packing, porosity, and water saturation were radially uniform, and a 1-D cylindrical mesh was generated to describe the sample. Along the z-axis, the mesh was discretized into 18 subdivisions of a uniform thickness $\Delta z = 5$ mm. This is identical to the x-ray CT scanning slice thickness. Each subdivision has a volume of $5.611 \times 10^{-6} \text{ m}^3$ and a contact area of $1.122 \times 10^{-3} \text{ m}^2$ with neighboring slices. Since there is no hydraulic interaction or thermal disturbance across the rubber sleeve, no grid was defined outside of the sample.

Porosity and initial water saturation estimated by CT images were individually averaged for each slice and incorporated into the model by assigning the values to each corresponding subdivision of the mesh. The two observation locations for each test selected for water saturation estimation were used in the calibrations. Because of the variability in the initial conditions (hydrate saturation and porosity), the two observation locations were calibrated separately to estimate relative permeability functions for the specific sample segments.

Boundary and Initial Conditions

All the same experimental conditions were applied to the simulations. The following boundary/initial conditions and assumptions were:

- A no-flow boundary condition was specified at the side boundary of the model, and a fixed-flux boundary condition was specified at the inlet element with the injection rate specified in the experiments ($Q = 0.1$ mL/min for Test 1 and 0.2 mL/min for Tests 2 and 3).
- Gravitational effects were not considered.
- Isothermal conditions were specified for the entire course of the waterflood (experiment conditions varied by 0.2C).
- Methane hydrate was assumed to be a stable solid phase under the specified pressure/temperature conditions. The calculated porosity and water saturations of the hydrate-bearing sand used in the simulations were based on this assumption. We refer to the water saturation calculated on this basis in this paper as S^* to denote the difference from a definition of water saturation that includes the hydrate as another partially pore-filling phase.

Modeling Approach

The relative permeability was estimated by calibrating simulated water saturations (S^*) at the two observation points for each test to measured values obtained from the CT image analysis. van Genuchten functions (van Genuchten 1980) were used for estimating relative permeability and capillary pressure. Even though the same parameter for the pore-size-distribution index (m) is included in both the relative permeability and capillary pressure functions, the parameter was separately calibrated for the relative permeability and capillary pressure function.

Tests 1 and 3 were used for calibration, because Test 2 exhibited unacceptably high heterogeneity in S_H . Permeabilities needed for the simulation were taken from the measured gas permeability values for the samples after hydrate was formed. Because Test 3 had about 86% conversion of water to hydrate, there was minimal water saturation in the sample before waterflooding. Residual and satiated water saturations of the hydrate-bearing sand sample were assumed to be 35% and 100%, respectively, and gas residual saturation was assumed to be 0%.

Each test had two observation locations; locations for Test 1 are at 57.5 mm (12th element, Location 460 on CT table) and at 82.5 mm (17th element, Location 435), and locations for Test 3 are at 7.5 mm (2nd element, Location 510) and at 72.5 mm (15th element, Location 445). Relative permeability parameters estimated at each observation location represent the relative permeability function of a sample section from the inlet point to the observation location. The two sections of each test sample were separately calibrated for relative permeability parameters because of different characteristics at each location.

Calibration was performed using TOUGH/iTOUGH2, an inverse modeling program (Pruess et al., 1996; Finsterle, 1999). The variation ranges of the van Genuchten parameters α and m were adapted from those reported by van Genuchten (1980) when considering the addition of the hydrate phase (Table 3).

RESULTS

Laboratory Measurements

Permeability

Table 2 lists the permeability values calculated for the tests performed including the gas permeability of the moist sand, the gas permeability of the sand with hydrate, and the saturated permeability. In Tests 1 and 2, permeability values of the hydrate-bearing systems are less than those of their corresponding moist sand initial condition.

In Test 1, the initial moist sand permeability was not measured at elevated pore pressure but with near atmospheric pore pressures. While the permeability of the system should not depend on pressure, the presence of air bubbles in the small diameter tubing leading to the differential pressure transducer could impact the transducer reading much more strongly under these conditions than under higher pressure conditions.

In Test 3, with the lowest initial water saturation, the permeability of the hydrate bearing sand was approximately the same as that of the moist sand. Following the gas permeability measurement of the moist sand in Test 3, additional gas was flowed through the sample prior to hydrate formation. This additional gas flow could have altered the water configuration in the sample, and the resulting hydrate uniformity causing the permeability of the hydrate-bearing sand to be slightly higher than the moist sand.

Table 2. Permeability values for the studied conditions

Test	$S_W/S_H/S_G$	Fluid	Perm. (m ²)	Std. Dev.
1	0.53/0.00/0.47	G	1.748E-12	2.137E-13
1	0.00/0.58/0.42	G	7.387E-14	1.432E-14
1	0.42/0.58/0.00	W	6.234E-15	
1	1.00/0.00/0.00	W	3.935E-13	6.362E-14
2	0.41/0.00/0.59	G	1.217E-13	1.774E-14
2	0.00/0.44/0.56	G	4.863E-14	5.792E-15
2	1.00/0.00/0.00	W	3.935E-13	6.362E-14
3	0.19/0.19/0.81	G	2.157E-13	6.047E-14
3	0.03/0.18/0.79	G	2.729E-13	9.357E-14
3	1.00/0.00/0.00	W	2.530E-12	9.596E-13

G: gas, W: water, H: hydrate, S: saturation

Waterflooding experiments

Water was introduced into the samples at fixed rates ($Q = 0.1$ mL/min in Test 1, and $Q = 0.2$ mL/min in Tests 2 and 3), and the evolution of phase saturations at specific locations were monitored using CT. The average saturation (S^*) determined from the CT data for each of the monitored locations over the duration of the water floods and the differential pressures across the sample for the same duration are shown in Figure 3. Comparing the three graphs, the highest pressure differentials occur in Test 1, with the highest initial water and resulting hydrate saturations. The maximum pressure differential decreases with decreasing initial water saturation (and lower resulting hydrate saturations). In Test 1, the differential pressure increases greatly over the test duration compared to the other two tests. It is thought that increased hydrate saturation near the outlet is responsible for this differential pressure increase.

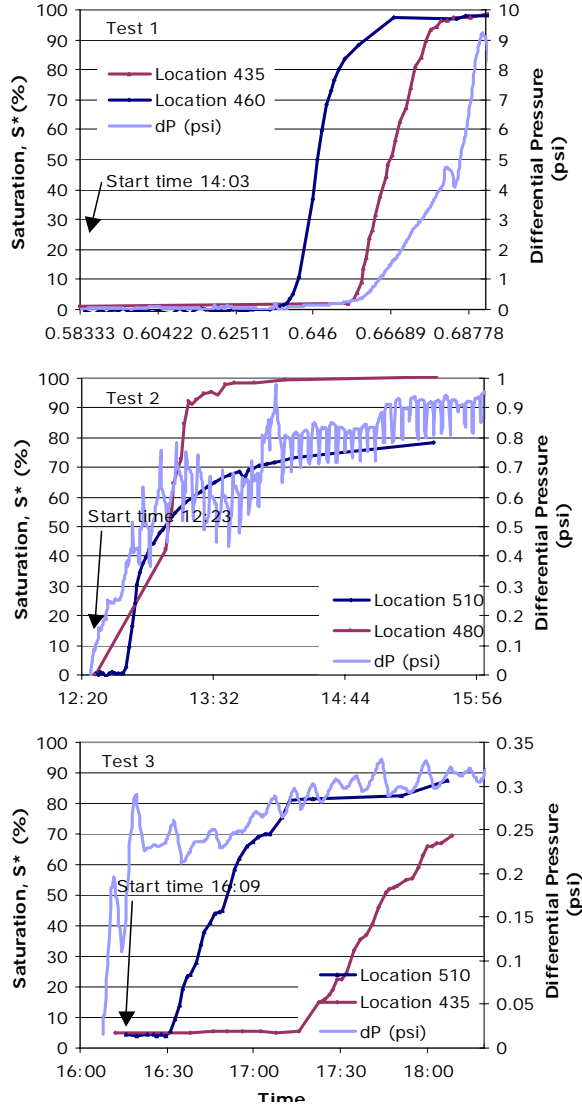


Figure 3. Average saturation (S^*) at the indicated locations and differential pressure across the sample.

CT images during water flooding show that water flows initially through preferential flow pathways when high porosity is available, and then begins to flow into the higher hydrate saturation region (Figure 4). Hydrate formation seems block pores and hinder water from flowing through the hydrate formation. Because the hydrate distribution is not uniform, the preferential flow pattern would be inevitable.

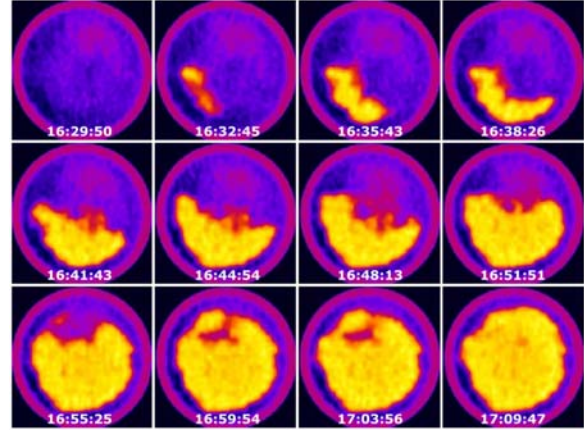


Figure 4. CT images at Location 510 of Test 3. Yellow region shows water front advance.

Numerical Calibration

Calibration results for Tests 1 and 3 are plotted in Figure 5 and the estimated relative permeability parameters are listed in Table 3. Table 3 also lists hydrate saturation and porosity with section averages. Note that there is a significant saturation difference variation between the specific and the average section values in Test 1.

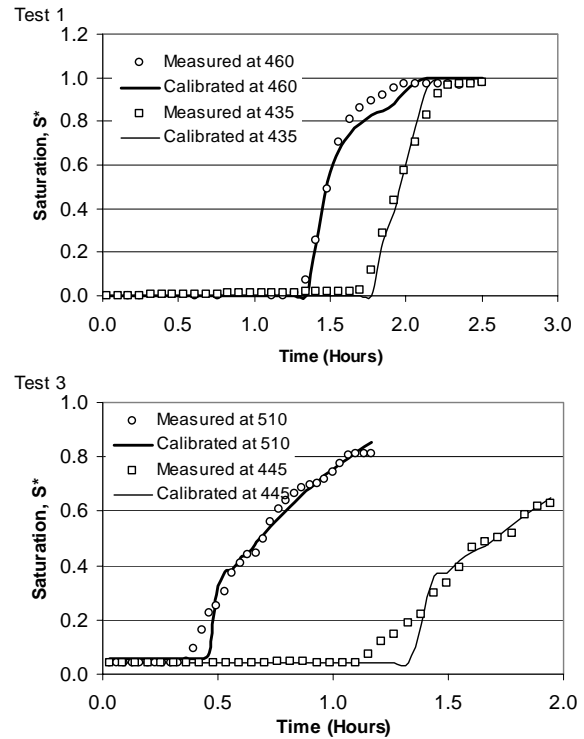


Figure 5. Calibration of water saturation (S^*) against measured water saturations (S^*) at two observation locations for Tests 1 and 3.

The estimated parameters for the two locations in each test were not identical, and consistency in the estimated parameters was not observed between the Tests 1 and 3. Interpretation of these data would be more meaningful if measured values were available to replace assumptions and simplifications, such as the assumed uniform hydrate saturation distribution and assumed constant residual saturation of water and gas. Reducing uncertainty in measurements of water saturation and core volume with the CT scans would also improve data quality.

Table 3. Measured hydrate saturation and porosity and calibrated van Genuchten parameters

Test	Test 1		Test 3	
Location	460	435	510	445
	(Location/Section Average)			
S _H	0.77/0.60	0.85/0.67	0.30/0.30	0.24/0.26
Porosity	0.09/0.16	0.06/0.13	0.28/0.28	0.29/0.29
m (R.P.)	0.78	0.55	0.94	0.80
m (C.P.)	0.68	0.83	0.90	0.38
α [1/p]	2.51×10^{-4}	1.58×10^{-5}	9.66×10^{-6}	3.24×10^{-3}

R.P.: relative permeability, C.P.; capillary pressure

SUMMARY AND CONCLUSIONS

This report describes preliminary estimates of relative permeability parameters for gas and water through methane hydrate-bearing sand. X-ray CT was used nondestructively to quantify the water and hydrate saturations inside the sample, and an inversion simulation technique was used to estimate the van Genuchten α and m parameters by calibrating simulated water saturations to CT-measured water saturations during a waterflood. This technique to derive the relative permeability function in gas hydrate-bearing sediments is the first attempt of its kind, and the results suggest that the technique may be a way to estimate relative permeability functions especially with improvements to experimental design.

The estimated relative permeability parameters are not unique. The hydrate distribution revealed by the x-ray CT is heterogeneous despite relatively uniform initial water saturation and porosity distribution. Therefore, the CT-measured available pore space for flow is critical information. The assumption that the sample is uniform in terms of hydrate saturation and water flow path distribution can be problematic.

The tests and subsequent modeling provided a series of important observations, including the first quantification of non-uniformity of hydrate formation in a porous medium with a continuous gas phase under a confining pressure. These tests also provide the first visualization of water flow through a hydrate-bearing porous medium with heterogeneous

hydrate saturation. The modeling has provided us with needed information although measurement uncertainty should be reduced, and the technique improved.

ACKNOWLEDGMENTS

This work was supported, in part, through Work for Others Agreement No. LB05001888 between the Regents of the University of California as the Management and Operating Contractor for the Ernest Orlando Lawrence Berkeley National Laboratory (Berkeley Lab) Operating Under Prime Contract No. DE-AC03-76SF00098 for the U.S. Department of Energy and the Korean Institute of Geoscience and Mineral Resources (KIGAM).

REFERENCES

- Finsterle, S., *iTOUGH2 User's guide*. LBNL-40040, Lawrence Berkeley National Laboratory, Berkeley, CA, 1999.
- Kneafsey, T.J., L. Tomutsa, C.E. Taylor, A. Gupta, A. G. Moridis, B. Freifeld, and Y. Seol, Methane hydrate formation and dissociation in partially saturated sand, 229th ACS National Meeting, San Diego, CA, 2005.
- Pruess, K., A. Simmons, Y.S. Wu, and G. Moridis, *TOUGH2 Software Qualification*, Lawrence Berkeley National Laboratory, Report LBNL-38383, Berkeley, CA, 1996.
- Tomutsa, L., B. Freifeld, T.J. Kneafsey, and L.A. Stern, X-ray computed tomography observation of methane hydrate dissociation, SPE Gas Technology Symposium, Calgary, Alberta, Canada, 2002.
- van Genuchten, M. Th, A closed-form equation for predicting the hydraulic conductivity of unsaturated soils, *Soil Sci. Soc. Am. J.*, 44: 892-898, 1980.